3290 *Chem. Mater.* **2010,** *22,* 3290–3299
DOI:10.1021/cm100661z

CHEMISTRY OF MATERIALS
Article

New Two-Dimensional Thiophene−Acceptor Conjugated Copolymers for Field Effect Transistor and Photovoltaic Cell Applications

Jung-Hsun Tsai,[†] Wen-Ya Lee,[†] Wen-Chang Chen,*[,†,‡] Chao-Ying Yu,[§] Gue-Wuu Hwang,[§] and Ching Ting*[,§]

[†]*Department of Chemical Engineering, National Taiwan University, Taipei 106, Taiwan,* [‡]*Institute of Polymer Science and Engineering, National Taiwan University, Taipei 106, Taiwan, and* [§]*Materials and Chemical Laboratories, Industrial Technology Research Institute, Hsinchu 300, Taiwan*

Received March 4, 2010. Revised Manuscript Received April 15, 2010

We report the synthesis, properties, and optoelectronic device applications of two-dimensional (2D) like conjugated copolymers, **P4TBT**, **P4TDTBT**, **P4TDTQ**, and **P4TDPP**, consisting of 2′,5″-bis-(trimethystannyl)-5,5‴-di-(2-ethylhexyl)[2,3′;5′,2″;4″,2‴]quarterthiophene (**4T**) with the following four acceptors of 4,7-dibromo-2,1,3-benzothiodiazole (**BT**), 4,7-di-2-thienyl-2,1,3-benzothiadiazole (**DTBT**), 2,3-bis(4-(2-ethylhexyloxy)phenyl)-5,8-bis[5′-bromodithien-2-ylquinoxalines] (**DTQ**), and 3,6-bis(5-bromothiophen-2-yl)-2,5-bis(2-ethylhexyl)pyrrolo[3,4-*c*]pyrrole-1,4-dione (**DPP**). The optical band gaps (eV) of the studied conjugated copolymers are in the order of **P4TDPP** (1.29) < **P4TDTBT** (1.60) < **P4TDTQ** (1.83) < **P4TBT** (1.88). The 2D-like conjugated copolymers exhibited high field effect (FET) hole mobilities in the range of $10^{-1}-10^{-4}$ cm^2 V^{-1} s^{-1}. On the other hand, the FET electron mobilities were observed for **P4TDTBT** and **P4TDPP** because of their relatively low-lying LUMO level suitable for electron injection. In particular, **P4TDPP** showed the ambipolar characteristics with the hole and electronic mobilities of 0.115 cm^2 V^{-1} s^{-1} (on/off ratio: 2.49×10^4) and 3.08×10^{-3} cm^2 V^{-1} s^{-1} (on/off ratio: 7.34×10^2), respectively, which was strongly related to its ordered intermolecular chain packing based on the DSC and XRD results. The power conversion efficiencies (PCE) of the prepared polymer/$PC_{71}BM$ (1:3) based photovoltaic cells were in the range 1.28−1.67% under the illumination of AM 1.5G (100 mW/cm^2). The PCE could be enhanced up to 2.43% of the **P4TDPP**/$PC_{71}BM$ (1:2) based device because of the balanced hole/electron mobility. The above results indicate that these two-dimensional **4T**−acceptor conjugated copolymers could enhance the charge-transport characteristics and are promising materials for organic optoelectronic devices.

Introduction

Donor−acceptor (D−A) conjugated copolymers have attracted extensive scientific interest because their electronic and optoelectronic properties could be efficiently tuned through intramolecular charge transfer (ICT).[1,2] Various device applications have been explored for such conjugated copolymers, including light emitting diodes (LED),[3−7] photovoltaic cells (PV),[8−46] and field-effect transistors (FET).[47−62] The electron-rich donors of fluorene,[3−7,22] thiophene,[25−27,51−57] carbazole,[39−42]

*To whom correspondence should be addressed. E-mail: chenwc@ntu.edu.tw; cting@itri.org.tw.

(1) van Mullekom, H. A. M.; Vekemans, J. A. J. M.; Havinga, E. E.; Meijer, E. W. *Mater. Sci. Eng. R.* **2001**, *32*, 1.
(2) Tsai, F. C.; Chang, C. C.; Liu, C. L.; Chen, W. C.; Jenekhe, S. A. *Macromolecules* **2005**, *38*, 1958.
(3) Ego, C.; Marsitzky, D.; Becker, S.; Zhang, J.; Grimsdale, A. C.; Mullen, K.; MacKenzie, J. D.; Silva, C.; Friend, R. H. *J. Am. Chem. Soc.* **2003**, *125*, 437.
(4) Liu, J.; Guo, X.; Bu, L. J.; Xie, Z. Y.; Cheng, Y. X.; Geng, Y. H.; Wang, L. X.; Jing, X. B.; Wang, F. S. *Adv. Funct. Mater.* **2007**, *17*, 1917.
(5) Wu, W. C.; Liu, C. L.; Chen, W. C. *Polymer* **2006**, *47*, 627.
(6) Peng, Q.; Peng, J. B.; Kang, E. T.; Neoh, K. G.; Cao, Y. *Macromolecules* **2005**, *38*, 7292.
(7) Yang, R. Q.; Tian, R. Y.; Yan, J. G.; Zhang, Y.; Tang, J.; Hou, Q.; Yang, W.; Zhang, C.; Cao, Y. *Macromolecules* **2005**, *38*, 244.
(8) Dennler, G.; Scharber, M. C.; Ameri, T.; Denk, P.; Forberich, K.; Waldauf, C.; Brabec, C. J. *Adv. Mater.* **2008**, *20*, 579.
(9) Scharber, M. C.; Muhlbacher, D.; Koppe, M.; Denk, P.; Walfauf, C.; Heeger, A. J.; Brabec, C. J. *Adv. Mater.* **2007**, *18*, 794.
(10) Coakley, K. M.; McGehee, M. D. *Chem. Mater.* **2004**, *16*, 4533.
(11) Chen, C. P.; Chan, S. H.; Chao, T. C.; Ting, C.; Ko, B. T. *J. Am. Chem. Soc.* **2008**, *130*, 12828.
(12) Chan, S. H.; Chen, C. P.; Chao, T. C.; Ting, C.; Lin, C. S.; Ko, B. T. *Macromolecules* **2008**, *41*, 5519.
(13) Yu, C. Y.; Chen, C. P.; Chan, S. H.; Hwang, G. W.; Ting, C. *Chem. Mater.* **2009**, *21*, 3262.
(14) Lu, J.; Liang, F.; Drolet, N.; Ding, J.; Tao, Y.; Movileanu, R. *Chem. Commun.* **2008**, 5315.
(15) Tsai, J. H.; Chueh, C. C.; Chen, Lai, M. H.; Wang, C. F.; Chen, W. C.; Ko, B. T.; Ting, C. *Macromolecules* **2009**, *42*, 1897.
(16) Lai, M. H.; Chueh, C. C.; Chen, W. C.; Wu, J. L.; Chen, F. C. *J. Polym. Sci., Part A: Polym. Chem.* **2009**, *47*, 973.
(17) Li, G.; Shrotriya, V.; Huang, J.; Yao, Y.; Moriarty, T.; Emery, K.; Yang, Y. *Nat. Mater.* **2005**, *4*, 864.
(18) Kim, Y.; Cook, S.; Tuladhar, S. M.; Choulis, S. A.; Nelson, J.; Durrant, J. R.; Bradley, D. D. C.; Giles, M.; Mcculloch, I.; Ha, C. S.; Ree, M. *Nat. Mater.* **2006**, *5*, 197.
(19) Peet, J.; Kim, J. Y.; Coates, N. E.; Ma, W. L.; Moses, D.; Heeger, A. J.; Bazan, G. C. *Nat. Mater.* **2007**, *6*, 497.
(20) Wong, W. Y.; Wang, X. Z.; He, Z.; Djurisic, A. B.; Yip, C. T.; Cheung, K. Y.; Wang, H.; Mak, C. S. K.; Chan, W. K. *Nat. Mater.* **2007**, *6*, 521.
(21) Campos, L. M.; Tontcheva, A.; Gunes, S.; Sonmez, G.; Neugebauer, H.; Sariciftci, N. S.; Wudl, F. *Chem. Mater.* **2005**, *17*, 4031.
(22) Gadisa, A.; Mammo, W.; Andersson, L. M.; Admassive, S.; Zhang, F.; Andersson, M. R.; Inganäs, O. *Adv. Funct. Mater.* **2007**, *17*, 3836.
(23) Hou, J. H.; Park, M. H.; Zhang, S. Q.; Yao, Y.; Chen, L. M.; Li, J. H.; Yang, Y. *Macromolecules* **2008**, *41*, 6012.

 Published on Web 04/23/2010

cyclopentadithiophene,[24,25] and benzodithiophene[28,46] were used as the building block in the D−A conjugated copolymers for the device applications, especially PV and FET. We reported several donor based D−A conjugated copolymers and demonstrated the significance of donor−acceptor strength and backbone coplanarity on the electronic and optoelectronic properties, including thiophene/phenylene/thiophene (**TPT**),[11−13] indolocarbazole,[15] and dialkoxylphenylene.[53]

Most of the above-reported D−A conjugated copolymers focused on the main chain system. Recently, two-dimensional (2D) like conjugated polymers with conjugated side chains have been developed to enhance charge transport as well as their device performance.[29−38,46] Pioneering works done by Li and his co-workers concluded that the incorporation of conjugated side chains into polythiophene significantly broadened the absorption spectrum and enhanced the power conversion efficiencies of photovoltaic cells, such as bi(phenylenevinylene),[29] bi(thienylenevinylene),[30,31] and phenothiazinevinylene.[32] In addition, the cross-linked polythiophene derivatives with conjugated bridges were shown to have high charge carrier mobility.[33] Unlike the bi(thienylenevinylene) system,[30] we employed the alkylthiophenes directly attached onto the polythiophene backbone without the vinylene linkers.[34] Such polymers had the lower band gap of 1.77 eV and relatively low-lying HOMO levels (−5.46 to −5.62 eV) in comparison with those of parent P3HT system,[34] indicating the better absorption ability and air stability for solar cell devices. Very recently, the similar structures with less densely conjugated side chains compared to our previous work[34] were found to have a high hole mobility of 5.1×10^{-2} cm^2 V^{-1} s^{-1}.[35] Other examples employed 2D-like conjugated copolymers, including polythiophene with an electron-withdrawing phenanthrenylimidazole side chain[36−38] and 4,7-bis(2-thienyl)-2,1,3 -benzothiadiazole-5,5′-diyl with a conjugated alkylthiophene side chain.[46] These copolymers showed the extent of conjugation, high PV efficiency,[34,60] and large charge carrier mobility.[31,35−38] The above reports suggest that 2D-like conjugated polymer systems have emerged as a promising candidate for the donor building block. However, the synthesis and properties of 2D-like donor−acceptor conjugated copolymers have not been fully explored yet.

Herein we report the synthesis, properties, and optoelectronic device applications of four poly(**4T**−acceptor) derivatives, including poly[2′,5″-5,5‴-di-(2-ethylhexyl)-[2,3′;5′,2″;4″,2‴]quaterthiophene-*alt*-4,7-(2,1,3-benzothiadiazole)] (**P4TBT**), poly[2′,5″-5,5‴-di-(2-ethylhexyl)-[2,3′;5′,2″;4″,2‴]-quaterthiophene-*alt*-4,7-dithien-2-yl-2,1,3-benzothiadiazole] (**P4TDTBT**), poly[2′,5″-5,5‴-di-(2-ethylhexyl)[2,3′;5′,2″;4″,2‴]quaterthiophene-*alt*-2,3-bis[4-(2-ethylhexyloxy)phenyl)-5,8-dithien-2-yl-quinoxaline] (**P4TDTQ**), and poly[2′,5″-5,5‴-di-(2-ethylhexyl)-[2,3′;5′,2″;4″,2‴]quaterthiophene-*alt*-3,6-dithien-2-yl-2,5-di(2-ethylhexyl)pyrrolo[3,4-*c*]pyrrole-1,4-dione-5′,5″-diyl] (**P4TDPP**). These polymers were synthesized by Stille coupling reaction under microwave heating, as shown in Scheme 1. The polymer carrier mobility was obtained from the top-contact/bottom-gate field effect transistor (FET) devices and correlated with the acceptor strength,

(24) Soci, C.; Hwang, I. W.; Moses, D.; Zhu, Z.; Waller, D.; Gaudiana, R.; Brabec, C. J.; Heeger, A. J. *Adv. Funct. Mater.* **2007**, *17*, 632.
(25) Moulé, A. J.; Tsami, A.; Bünnagel, T. W.; Forster, M.; Kronenberg, N. M.; Scharber, M.; Koppe, M.; Morana, M.; Brabec, C. J.; Meerholz, K.; Scherf, U. *Chem. Mater.* **2008**, *20*, 4045.
(26) Okamota, T.; Jiang, Y.; Qu, F.; Mayer, A. C.; Parmer, J. E.; McGehee, M. D.; Bao, Z. *Macromolecules* **2008**, *41*, 6977.
(27) Baek, N. S.; Hau, S. K.; Yip, H. L.; Acton, O.; Chen, K. S.; Jen, A. K. Y. *Chem. Mater.* **2008**, *20*, 5734.
(28) Liang, Y. Y.; Feng, D. Q.; Wu, Y.; Tsai, S. T.; Li, G.; Ray, C.; Yu, L. P. *J. Am. Chem. Soc.* **2009**, *131*, 56.
(29) Hou, J. H.; Huo, L. J.; He, C.; Yang, C. H.; Li, Y. F. *Macromolecules* **2006**, *39*, 594.
(30) Hou, J. H.; Tan, Z. A.; Yan, Y.; He, Y. J.; Yang, Y. F.; Li, Y. F. *J. Am. Chem. Soc.* **2006**, *128*, 4911.
(31) Li, Y. F.; Zou, Y. P. *Adv. Mater.* **2008**, *20*, 2952.
(32) Zou, Y. P.; Wu, W. P.; Sang, G. Y.; Yang, Y.; Liu, Y. Q.; Li, Y. F. *Macromolecules* **2007**, *40*, 7231.
(33) Zhou, E. J.; Tan, Z.; Yang, Y.; Hou, L. J.; Zou, Y. P.; Yang, C. H.; Li, Y. F. *Macromolecules* **2007**, *40*, 1831.
(34) Yu, C. Y.; Ko, B. T.; Ting, C.; Chen, C. P. *Sol. Energy Mater. Sol. Cells* **2009**, *93*, 613.
(35) Park, J. W.; Lee, D. H.; Chung, D. S.; Kang, D. M.; Kim, Y. H.; Park, C. E.; Kwon, S. K. *Macromolecules* **2010**, *43*, 2118.
(36) Chang, Y. T.; Hsu, S. L.; Su, M. H.; Wei, K. H. *Adv. Funct. Mater.* **2007**, *17*, 3326.
(37) Chang, Y. T.; Hsu, S. L.; Chen, G. Y.; Su, M. H.; Singh, T. A.; Diau, E. W. G.; Wei, K. H. *Adv. Funct. Mater.* **2008**, *18*, 2356.
(38) Chang, Y. T.; Hsu, S. L.; Su, M. H.; Wei, K. H. *Adv. Mater.* **2009**, *21*, 2093.
(39) Blouin, N.; Michaud, A.; Leclerc, M. *Adv. Mater.* **2007**, *19*, 2295.
(40) Blouin, N.; Michaud, A.; Gendron, D.; Wakim, S.; Blair, E.; Neagu-Plesu, R.; Belletete, M.; Durocher, G.; Tao, Y.; Leclerc, M. *J. Am. Chem. Soc.* **2008**, *130*, 732.
(41) Zou, Y. P.; Gendron, D.; Ach, R. B.; Najari, A.; Tao, Y.; Leclerc, M. *Macromolecules* **2009**, *42*, 2891.
(42) Qin, R. P.; Li, W. W.; Li, C. H.; Du, C.; Veit, C.; Schleiermacher, H. F.; Andersson, M.; Bo, Z. S.; Liu, Z. P.; Inganäs, O.; Wuerfel, U.; Zhang, F. L. *J. Am. Chem. Soc.* **2009**, *131*, 14612.
(43) Zhou, E.; Yamakawa, S.; Tajima, K.; Yang, C.; Hashimoto, K. *Chem. Mater.* **2009**, *21*, 4055.
(44) Hou, L. J.; Hou, J. H.; Chen, H. Y.; Zhang, S. Q.; Yang, J.; Chen, T. L.; Yang, Y. *Macromolecules* **2009**, *42*, 6564.
(45) Bijleveld, J. C.; Zoombelt, A. P.; Mathijssen, S. G. J.; Wienk, M. M.; Turbiez, M.; de Leeuw, D. M.; Janssen, R. A. J. *J. Am. Chem. Soc.* **2009**, *131*, 16616.
(46) Huo, L.; Hou, J.; Zhang, S.; Chen, H. Y.; Yang, Y. *Angew Chem., Int. Ed.* **2010**, *49*, 1500.
(47) Sirringhaus, H.; Tessler, N.; Friend, R. H. *Science* **1998**, *280*, 1741.
(48) Chua, L. L.; Zaumseil, J.; Chang, J. F.; Ou, E. C.; Ho, P. K. H.; Sirringhaus, H.; Friend, R. H. *Nature* **2005**, *434*, 194.
(49) Gadisa, A.; Perzon, E.; Andersson, M. R.; Inganäs, O. *Appl. Phys. Lett.* **2007**, *90*, 113510.
(50) Yan, H.; Chen, Z. H.; Zheng, Y.; Newman, C.; Quinn, J. R.; Dotz, F.; Kastler, M.; Facchetti, A. *Nature* **2009**, *457*, 679.
(51) Lee, W. Y.; Cheng, K. F.; Wang, T. F.; Chueh, C. C.; Chen, W. C.; Tuan, C. S.; Lin, J. L. *Macromol. Chem. Phys.* **2007**, *208*, 1919.
(52) Cheng, K. F.; Liu, C. L.; Chen, W. C. *J. Polym. Sci., Part A: Polym. Chem.* **2007**, *45*, 5872.
(53) Liu, C. L.; Tsai, J. H.; Lee, W. Y.; Chen, W. C.; Jenekhe, S. A. *Macromolecules* **2008**, *41*, 6952.
(54) Yamamoto, T.; Kukubo, H.; Kobashi, M.; Sakai, Y. *Chem. Mater.* **2004**, *16*, 4616.
(55) Champion, R. D.; Cheng, K. F.; Pai, C. L.; Chen, W. C.; Jenekhe, S. A. *Macromol. Rapid Commun.* **2005**, *26*, 1835.
(56) Babel, A.; Zhu, Y.; Cheng, K. F.; Chen, W. C.; Jenekhe, S. A. *Adv. Funct. Mater.* **2007**, *17*, 2542.
(57) Zhu, Y.; Champion, R. D.; Jenekhe, S. A. *Macromolecules* **2006**, *39*, 8712.
(58) Becerril, H. A.; Miyaki, N.; Tang, M. L.; Mondal, R.; Sun, Y. S.; Mayer, A. C.; Parmer, J. E.; McGehee, M. D.; Bao, Z. *J. Mater. Chem.* **2009**, *19*, 591.
(59) Zaumseil, J.; Sirringhaus, H. *Chem. Rev.* **2007**, *107*, 1296.
(60) Bao, Z.; Locklin, J. *Organic Field-Effect Transistors*; CRC Press: Boca Raton, FL, 2007.
(61) Morana, M.; Koers, P.; Waldauf, C.; Koppe, M.; Muehlbacher, D.; Denk, P.; Scharber, M.; Waller, D.; Brabec, C. *Adv. Funct. Mater.* **2007**, *17*, 3274.
(62) Morana, M.; Wegscheider, M.; Bonanni, A.; Kopidakis, N.; Shaheen, S.; Scharber, M.; Zhu, Z.; Waller, D.; Gaudiana, R.; Brabec, C. *Adv. Funct. Mater.* **2008**, *18*, 1757.

Scheme 1. Preparation of the 4T-Based Donor−Acceptor Conjugated Copolymers

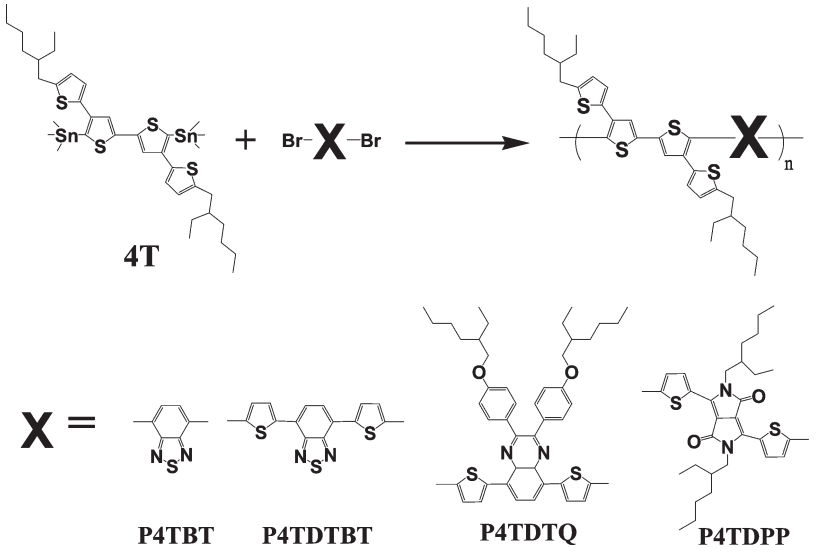

molecular energy levels, and morphology. Polymer solar cell devices were fabricated by spin-coating a polymer blend of **4T**−acceptor copolymer/$PC_{71}BM$ sandwiched between a transparent anode (ITO) and cathodes (Ca/Al). The balanced hole and electron mobility were also explored to optimize the performance of **P4TDPP**-based solar cell device. Our experimental results indicated that the poly(**4T**−acceptor) copolymers are promising candidates for high performance FET or PV devices.

Experimental Section

Materials. Tri(*o*-tolyl)phosphine, tris(dibenzylideneacetone)dipalladium(0), trimethyl(thiophen-2-yl)stannane, and bromothiophene were purchased from Aldrich (MO) and used without further purification. Common organic solvents for synthesis and ultraanhydrous solvents (such as chloroform, chlorobenzene, and *o*-dichlorobenzene) for device applications were purchased from Tedia (OH) and Aldrich (MO), respectively. The donor of 2′,5″-bis(trimethystannyl)-5,5‴-di-(2-ethylhexyl)-[2,3′;5′,2″;4″,2‴]quaterthiophene (**4T**) was synthesized according to our previous work.[34] The following acceptor and donor−acceptor−donor blocks were prepared according to literature procedures: 4,7-dibromo-2,1,3-benzothiodiazole (**BT**),[5] 4,7-di-2-thienyl-2,1,3-benzothiadiazole (**DTBT**),[53] 2,3-bis(4-(2-ethylhexyloxy)phenyl)-5,8-bis[5′-bromodithien-2-yl-quinoxalines] (**DTQ**),[16] 3,6-bis(5-bromothiophen-2-yl)-2,5-bis(2-ethylhexyl)-pyrrolo[3,4-*c*]pyrrole-1,4-dione (**DPP**).[43] 1-(3-Methoxycarbonyl)-propyl-1-phenyl[6,6]C-71 ($PC_{71}BM$) was purchased from Solenne (Groningen, The Netherlands) for solar cell device application. The surface treatment agents of octyltrichlorosilane (OTS), octadecyltrichlorosilane (ODTS), and phenyltrichlorosilane (PTS) were purchased from Acros (Geel, Belgium) for field-effect transistor characterization.

General Procedures for Polymerization. The general procedure of synthesizing **4T**−acceptor conjugated copolymers is shown in Scheme 1. 2′,5″-Bis(trimethystannyl)-5,5‴-di-(2-ethylhexyl)[2,3′;5′,2″;4″,2‴]quaterthiophene (**4T**), dibromo monomers (**BT**, **DTBT**, **DTQ**, or **DPP**), tri(*o*-tolyl)phosphine (16 mol % with respect to ditin monomer), and tris(dibenzylideneacetone)dipalladium(0) (2 mol % with respect to ditin monomer) were dissolved in chlorobenzene, and these copolymers were synthesized by Pd(0)-catalyzed Stille coupling polymerization under microwave heating. After they were end-capped with trimethyl(thiophen-2-yl)stannane and bromothiophene (both 1.1 equiv with respect to ditin monomer), the mixture was cooled and poured into hexane. The precipitated material was dissolved into a small amount of $CHCl_3$ and then reprecipitated into methanol to afford a crude polymer. The crude polymer was washed for 24 h with acetone to remove oligomers and catalyst residues.

Poly[2′,5″-5,5‴-di-(2-ethylhexyl)[2,3′;5′,2″;4″,2‴]quaterthiophene-*alt*-4,7-(2,1,3-benzothiadiazole)] (P4TBT). Amounts of 722.2 mg (0.82 mmol) of **4T**, 239.3 mg (0.82 mmol) of **BT**, and 15 mL of chlorobenzene were used to afford a black solid (yield, 60%). ^{1}H NMR ($CDCl_3$), δ (ppm): 7.75−7.60 (br, Ar−H), 7.55−7.41 (br, Ar−H), 6.82−6.68 (br, Ar−H), 6.63−6.50 (br, Ar−H), 2.80−2.55 (br, Ar−CH_2), 1.49 (−CH), 1.40−1.15 (br, −CH_2), 1.05−0.70 (br, −CH_3). Anal. Calcd for [$C_{38}H_{42}N_2S_5$]: C, 66.43; H, 6.16; N, 4.08; S, 23.33. Found: C, 66.09; H, 5.88; N, 3.96; S, 21.49. Weight average molecular weight (M_w) and polydispersity index (PDI) estimated from GPC are 19670 g/mol and 1.57, respectively.

Poly[2′,5″-5,5‴-di-(2-ethylhexyl)[2,3′;5′,2″;4″,2‴]quaterthiophene-*alt*-4,7-dithien-2-yl-2,1,3-benzothiadiazole] (P4TDTBT). Amounts of 517.3 mg (0.59 mmol) of **4T**, 268.7 mg (0.59 mmol) of **DTBT**, and 15 mL of chlorobenzene were used to afford a black solid (yield, 63%). ^{1}H NMR ($CDCl_3$), δ (ppm): 8.10−6.35 (m, br, Ar−H), 3.05−2.40 (br, Ar−CH_2), 1.80−1.55 (br, −CH), 1.12−1.45 (br, −CH_2), 1.12−0.65 (br, −CH_3). Anal. Calcd for [$C_{46}H_{46}N_2S_7$]: C, 64.90; H, 5.45; N, 3.29; S, 26.37. Found: C, 64.53; H, 5.08; N, 3.22; S, 24.19. Weight average molecular weight (M_w) and polydispersity index (PDI) estimated from GPC are 26180 g/mol and 2.46, respectively.

Poly[2′,5″-5,5‴-di-(2-ethylhexyl)[2,3′;5′,2″;4″,2‴]quaterthiophene-*alt*-2,3-bis[4-(2-ethylhexyloxy)phenyl)-5,8-dithien-2-ylquinoxaline] (P4TDTQ). Amounts of 336.6 mg (0.38 mmol) of **4T**, 328.4 mg (0.38 mmol) of **DTQ**, and 10 mL of chlorobenzene were used to afford a black solid (yield, 70%). ^{1}H NMR ($CDCl_3$), δ (ppm): 8.15−6.50 (m, br, Ar−H), 3.95−3.70 (br, Ar−O−CH_2), 2.80−2.51 (br, Ar−CH_2), 1.81−1.62 (m, br, −CH), 1.62−1.05 (m, br, −CH_2), 1.05−0.60 (m, br, −CH_3). Anal. Calcd for [$C_{76}H_{90}N_2S_6$]: C, 72.68; H, 7.22; N, 2.23; S, 15.32. Found: C, 72.06; H, 6.89; N, 1.98; S, 14.22. Weight average molecular weight (M_w) and polydispersity index (PDI) estimated from GPC are 26590 g/mol and 2.02, respectively.

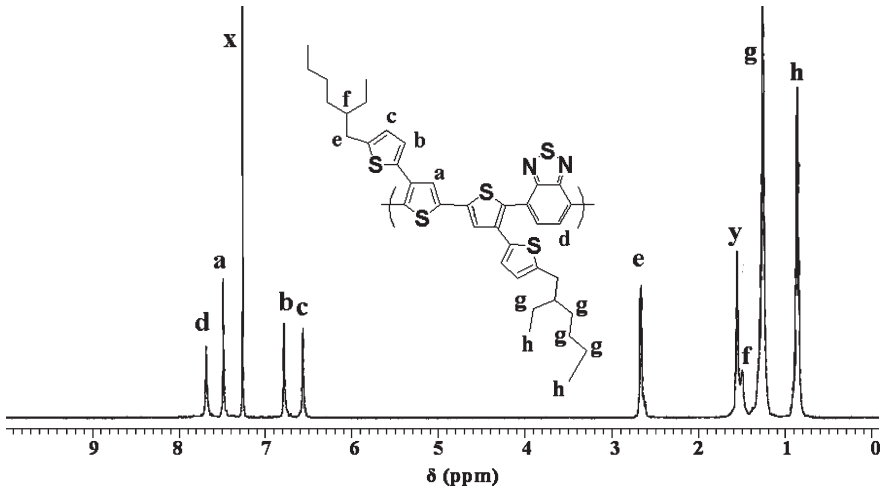

Figure 1. ^{1}H NMR spectrum of **P4TBT** in $CDCl_3$ (x = $CDCl_3$, y = H_2O).

Poly[2′,5″-5,5‴-di-(2-ethylhexyl)[2,3′;5′,2″;4″,2‴]quaterthiophene-*alt*-3,6-dithien-2-yl-2,5-di(2-ethylhexyl)pyrrolo[3,4-*c*]pyrrole-1,4-dione-5′,5″-diyl] (P4TDPP). Amounts of 591.2 mg (0.67 mmol) of **4T**, 455.8 mg (0.67 mmol) of **DPP**, and 15 mL of chlorobenzene were used to afford a black solid (yield, 65%). ^{1}H NMR ($CDCl_3$), δ (ppm): 9.25−8.90 (br, Ar−H), 7.47−6.45 (m, br, Ar−H), 4.15−3.60 (br, N−CH_2), 2.91−2.50 (m, br, Ar−CH_2) 1.95−1.55 (m, br, −CH), 1.49−1.05 (m, br, −CH_2), 1.05−0.65 (m, br, −CH_3). Anal. Calcd for [$C_{62}H_{78}N_2S_6$]: C, 69.23; H, 7.31; N, 2.60; S, 17.89. Found: C, 69.02; H, 7.05; N, 2.39; S, 17.44. Weight average molecular weight (M_w) and polydispersity index (PDI) estimated from GPC are 19310 g/mol and 1.91, respectively.

Characterization. ^{1}H NMR spectra were recorded with a Bruker Avance DRX 500 MHz instrument. Gel permeation chromatographic (GPC) analysis was performed on a Lab Alliance RI2000 instrument (two column, MIXED-C and D from Polymer Laboratories) connected to one refractive index detector from Schambeck SFD Gmbh. All GPC analyses were performed on polymer/THF solution at a flow rate of 1 mL/min at 40 °C and calibrated with polystyrene standards.

Thermogravimetric analysis (TGA) and differential scanning calorimetry (DSC) measurements were performed under a nitrogen atmosphere at a heating rate of 20 and 10 °C/min using a TA Instruments (TGA-951 and DSC-910S, respectively). X-ray diffraction (XRD) was performed by X'Pert PRO X-ray diffractometer using Cu Kα radiation (λ = 1.5418 Å) with a typical scan range of 2−30°, 0.1° step size, and 120 s per step on the drop-cast film.

UV−visible absorption spectra were recorded using a Hitachi U-4100 spectrophotometer. For the thin film spectra, polymers were first dissolved in dichlorobenzene (8 mg/mL), filtered through 0.45 μm pore size PTFE membrane syringe filters, and spin-coated at a speed rate of 1000 rpm for 60 s onto quartz substrate. Cyclic voltammetry (CV) was performed with the use of a three-electrode cell in which ITO (polymer film areas were about 0.5 × 0.7 cm^2) was used as a working electrode. A platinum wire was used as an auxiliary electrode. All cell potentials were taken with the use of a homemade Ag/AgCl, KCl (sat.) reference electrode.

Fabrication and Characterization of Field Effect Transistors. Highly doped n-type Si(100) wafers were used as substrates. A 300 nm SiO_2 layer (capacitance per unit area C_i = 10 nF cm^{-2}) as a gate dielectric was thermally grown onto the Si substrates. These wafers were cleaned in piranha solution, a 7:3 (v/v) mixture of H_2SO_4 and H_2O_2, rinsed with deionized water, and then dried by N_2. The phenyltrichlorosilane (PTS), octyltrichlorosilane (OTS), and octadecyltrichlorosilane (ODTS) treated surfaces on SiO_2/Si substrates were obtained by the following procedure: a clean SiO_2/Si substrate was immersed into a 10 mM solution of trichlorosilane in toluene at 80 °C overnight. Then the substrates were rinsed with toluene, acetone, isopropyl alcohol and dried with a steam of nitrogen. FET devices were deposited by spin-coating from chloroform, chlorobenzene, or 1,2-dichlorobenzene at a spin rate of 1000 rpm for 60 s. After drying, these samples were kept overnight at 70 °C to evaporate residue solvent. The top-contact source and drain electrodes were defined by 100 nm thick gold through a regular shadow mask, and the channel length (L) and width (W) were 50 and 1000 μm, respectively. FET transfer and output characteristics were recorded in a N_2-filled glovebox or in ambience by using a Keithley 4200 semiconductor parametric analyzer.

Fabrication and Characterization of Polymer Photovoltaic Cells. All the bulk-heterojunction photovoltaic cells and photodetectors were prepared using the same preparation procedures and device fabrication procedure as the following: The glass−indium tin oxide (ITO) substrates (obtained from Sanyo, Japan (8Ω/□) were first patterned by lithography, cleaned with detergent, ultrasonicated in acetone and isopropyl alcohol, subsequently dried on hot plate at 120 °C for 5 min, and finally treated with oxygen plasma for 5 min. Poly(3,4-ethylenedioxythiophene)/poly(styrene sulfonate) (PEDOT/PSS, Baytron P VP AI4083) was passed through a 0.45 μm filter before being deposited on ITO with a thickness of ∼30 nm by spin-coating at 3000 rpm in the air and dried at 140 °C for 1 h inside a glovebox. The thin film of the polymer/$PC_{71}BM$ blends on the top of the PEDOT/PSS layer was prepared by spin-coating from a dichlorobenzene solution. Subsequently the device was completed by evaporating 30 nm thickness of Ca and a 100 nm thickness of Al under $< 10^{-6}$ Torr pressure, respectively. The active area of the device is 4 mm^2.

Results and Discussion

Polymer Structure. The chemical structures of the synthesized polymers are confirmed by ^{1}H NMR and elemental analysis. Figure 1 shows the ^{1}H NMR spectrum of the polymer, **P4TBT**, in $CDCl_3$. For aromatic protons, the three peaks at 7.47 (peak a), 6.78 (peak b), and 6.56 (peak c) ppm are assigned to the protons on the thiophene rings of the **4T** unit, while the peak at 7.62 (peak d) ppm is assigned to the proton on the **BT** segment. Moreover, the

peaks at 2.80−2.55 ppm (thiophene−CH_2, peak e), 1.49 ppm (−CH, peak f), 1.40−1.15 ppm (−CH_2, peak g), and 1.05−0.70 ppm (−CH_3, peak h) are attributed to the ethylhexyl group in the **4T** unit, respectively. The number of aromatic and aliphatic protons estimated from the integration of peaks is in a good agreement with the proposed polymer structures. The ^{1}H NMR spectra of the other studied polymers are also consistent with the proposed polymer structures, as shown in Figures S2−S4 of the Supporting Information. Besides, the elemental analysis of the studied polymers exhibits a good agreement with the theoretical content. The above structural characterization results indicate the successful synthesis of the **4T**−acceptor conjugated copolymers.

All these polymers showed good solubility in common organic solvents such as chloroform, *o*-dichlorobenzene, and chlorobenzene. Hence, optical quality solution-processed thin films could be obtained by spin-coating for optoelectronic applications. The weight-averaged molecular weight and the polydispersity index (M_w, PDI) of the studied polymers, **P4TBT**, **P4TDTBT**, **P4TDTQ**, and **P4TDPP**, estimated by GPC are (19670, 1.57), (26180, 2.46), (26590, 2.02), and (19310, 1.91), respectively.

Thermal Stability. The glass transition temperature (T_g), melting temperature (T_m), and thermal decomposition temperature (T_d, 95 wt % residue) estimated from their differential scanning calorimetry (DSC, in Figure 2) and thermogravimetric analysis (TGA, in Figure S5 of the Supporting Information) curves are summarized in Table 1. The T_d values of all studied polymers are higher than 400 °C, which indicates their good thermal stability for optoelectronic devices. In our previous work,[34] the poly(**4T**−thiophene) did not show a clear thermal transition or melting point. However, the **4T**−acceptor copolymers exhibited a different thermal behavior. As shown in Figure 2, the T_g values of the **P4TBT**, **P4TDTBT**, and **P4TDTQ** are 55, 74, and 86 °C, respectively. The appearance of the phase transition could be attributed to the introduction of the ethylhexyl group into the **4T**−acceptor copolymers, which provides more free volume for polymer chain migration compared to poly(**4T**−thiophene) with the hexyl group.[34] Interestingly, **P4TBT** crystallizes when it is heated above the glass transition temperature (so-called cold crystallization), and the solid phase finally melts at ~250 °C. Compared with **P4TBT**, **P4TDTBT** shows a much higher T_g and the cold crystallization effect is quenched probably because of the high chain rigidity by the additional two thiophene moieties. On the other hand, **P4TDPP** has a crystalline melting temperature of ~283 °C and recrystallizes at ~243 °C. Such crystalline characteristics could be important for achieving high FET moiety, as discussed later.

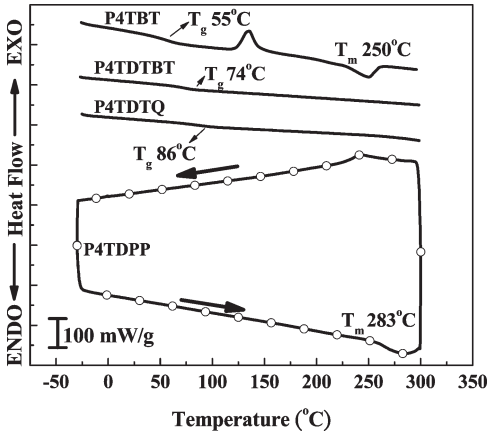

Figure 2. DSC curves of the studied copolymers at a heating rate of 10 °C/min under a nitrogen atmosphere.

Optical Properties. The UV−visible absorption spectra of the studied copolymers in dilute *o*-dichlorobenzene and thin films are shown in Figure 3a and Figure 3b, respectively. The corresponding maximum absorption wavelengths (λ_{max}), optical band gaps (E_g^{opt}), and absorption coefficients (α) are summarized in Table 1. The λ_{max} of **P4TBT**, **P4TDTBT**, **P4TDTQ**, and **P4TDPP** in solution are observed at 521, 566, 528, and 698 nm, respectively, while those of thin films are at 538, 606, 546, and 753 nm. The solid films show similar absorption spectra as *o*-dichlorobenzene solutions. However, the absorption spectra of **P4TDTBT** ($\Delta\lambda$ = 40 nm) and **P4TDPP** ($\Delta\lambda$ = 55 nm) are red-shifted compared with those of **P4TBT** ($\Delta\lambda$ = 17 nm) and **P4TDTQ** ($\Delta\lambda$ = 18 nm), suggesting the stronger $\pi-\pi$ interchain association and aggregation in the thin films of the former. Moreover, the thin films of **P4TBT** (1.07×10^5 cm^{-1} at $\lambda_{max} \approx 538$ nm), **P4TDTBT** (1.34×10^5 cm^{-1} at $\lambda_{max} \approx 606$ nm), **P4TDTQ** (1.10×10^5 cm^{-1} at $\lambda_{max} \approx 546$ nm), and **P4TDPP** (1.80×10^5 cm^{-1} at $\lambda_{max} \approx 753$ nm) exhibit moderate absorption coefficients comparable to that of the P3HT film (1.9×10^5 cm^{-1} at $\lambda_{max} \approx 552$ nm),[13] as shown in Figure 3b. The highest absorption coefficient of **P4TDPP** among all polymers is attributed to the incorporated **DPP** moiety[68] extensively used as industrial pigment.

The optical band gap (E_g^{opt}, eV) obtained from the extrapolation of the absorption edges on polymer films are in the order of **P4TDPP** (1.29) < **P4TDTBT** (1.60) < **P4TDTQ** (1.83) < **P4TBT** (1.88), which are significantly

Table 1. Optical and Electrochemical Properties of the Studied 4T-Based Donor−Acceptor Conjugated Copolymers

	UV−visible absorption spectra				cyclic voltammetry		
polymer	λ_{max} (sol.)[a] (nm)	λ_{max} (film)[a] (nm)	α[b] ($\times 10^5$ cm^{-1})	E_g^{opt} (eV)	E^{ox}_{onset}/HOMO (V/eV)	E^{red}_{onset}/LUMO (V/eV)	E_g^{ec} (eV)
P4TBT	521	538	1.07	1.88	1.20/−5.52	−1.05/−3.24	2.28
P4TDTBT	566	606	1.34	1.60	0.72/−5.04	−0.94/−3.38	1.66
P4TDTQ	528	546	1.10	1.83	0.96/−5.28	−1.10/−3.22	2.06
P4TDPP	698	753	1.80	1.29	0.85/−5.17	−0.67/−3.62	1.55

[a] *o*-Dichlorobenzene as processing solution. [b] Absorption coefficient (α) of the solid thin film at its maximum intensity of absorption peak ($\times 10^{-5}$ cm^{-1}).

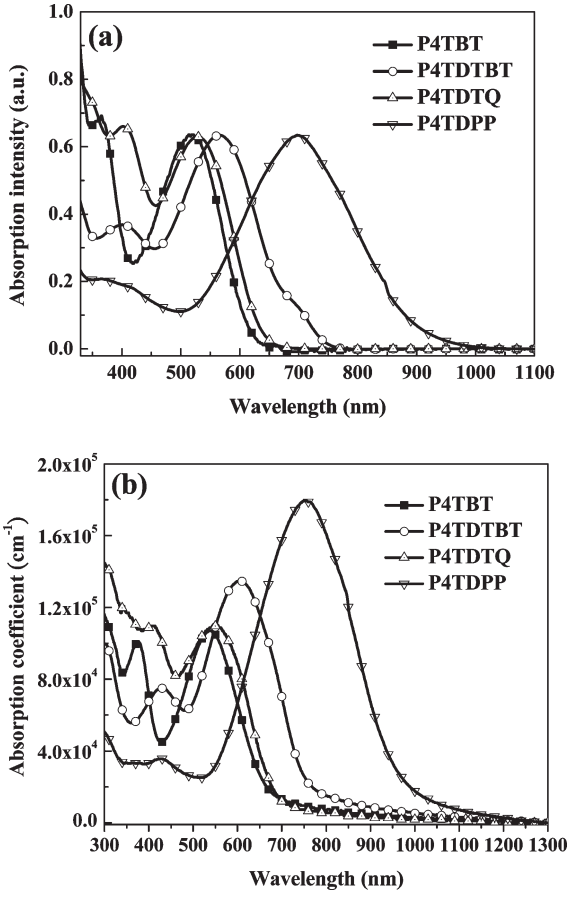

Figure 3. Optical absorption spectra of the studied copolymers in (a) dilute *o*-dichlorobenzene solutions and (b) thin films on a quartz plate.

lower than that of poly(**4T**−thiophene) of 1.98 eV.[34] The successfully reduced band gap is mainly due to the intramolecular charge transfer (ICT) effect between donor and acceptor. On the other hand, the incorporated bulky side chains (ethylhexyloxyphenyl or ethylhexyl) on acceptors could induce the twisted polymer backbone affecting the band gap. Therefore, the red-shifted absorption of **P4TDTBT** in comparison with that of **P4TBT** is related to the enhanced backbone coplanarity by incorporating the two thiophene moieties and the resulting intramolecular charge transfer.[51,53] The **BT** moiety has a stronger acceptor strength than the **Q**, which leads to the smaller E_g^{opt} of the **P4TDTBT** than that of the **P4TDTQ**. Besides, the smallest band gap of **P4TDPP** (1.29 eV) could be related to the planar and high conjugation of the **DPP** acceptor, which enhances the strong $\pi-\pi$ interactions and ICT among polymer main chain. The correlation of the optical band gap with the acceptor is consistent with our previous study on the thiophene−phenylene−thiophene/acceptor conjugated copolymers.[13]

Electrochemical Properties. Figure 4 shows the cyclic voltammetry (CV) curves of the studied polymers using polymer films in acetonitrile at a potential scan rate of 100 mV/s. The HOMO energy level, the LUMO energy level, and the electrochemical band gaps (E_g^{ec}) of the studied polymers were estimated from onset oxidation potentials ($E^{ox}{}_{onset}$) and onset reduction potentials ($E^{red}{}_{onset}$) based on the following equations: HOMO $= -[E^{ox}{}_{onset} - E^{ferrocene}{}_{1/2} + 4.8]$ V and

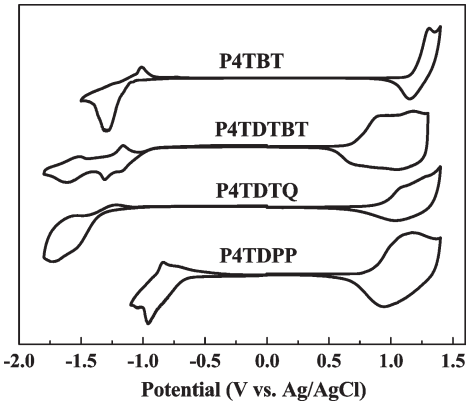

Figure 4. Cyclic voltammograms of the studied copolymers thin film in an acetonitrile solution of 0.1 M TBAP at a scan rate of 0.1 V/s.

LUMO $= -[E^{red}{}_{onset} - E^{ferrocene}{}_{1/2} + 4.8]$ V, where the potentials are referenced to an Ag/AgCl reference electrode. These relevant results are summarized at Table 1. Apparently, these studied polymers exhibit both reversible p-doping/dedoping (oxidation/rereduction) and n-doping/dedoping (reduction/reoxidation) processes. The corresponding HOMO energy levels of **P4TBT**, **P4DTBT**, **P4TDTQ**, and **P4TDPP** are −5.52, −5.04, −5.28, and −5.17 eV, respectively, while their LUMO energy levels are −3.24, −3.38, −3.22, and −3.62 eV. Although the band gap values have the same trend with the polymer structures, the E_g^{ec} values of the studied copolymers are 0.1−0.4 eV larger than the E_g^{opt} values, which is probably due to the exciton binding energy of conjugated polymers.[57] Compared to the HOMO/LUMO energy levels of **P4TBT** (−5.52/−3.24 eV), those of **P4TDTBT** (−5.04/−3.38 eV) exhibit a higher HOMO level by 0.48 eV and a lower LUMO level by 0.14 eV. The destabilization of HOMO and stabilization of LUMO level result in a reduced band gap of **P4TDTBT**, similar to those reported for the fluorene−**BT** conjugated copolymers.[63] It also demonstrates the significance of intramolecular charge transfer through the addition of two electron-donating thiophenes forming donor−acceptor−donor (D—A—D) structures. Among the studied copolymers, **P4TDPP** exhibits the lowest LUMO level (−3.62 eV) because of the strong electron affinity, which could be attributed to the existence of the electron-accepting lactam unit.[41,43,44] Note the reported **DPP**-based D—A copolymers with the LUMO levels at around −3.47 to −3.92 eV.[41,43,44] The above results indicate that the band gap and the molecular energy level of **4T**-based polymers can be efficiently tuned by incorporation with different electron-withdrawing (A) or D—A—D groups.

Polymer Field-Effect Transistor (FET) Characteristics. The FET characteristics obtained from these poly(**4T**−acceptor) derivatives are summarized in Table 2. The saturation-regime mobility was estimated from the slope of the plot of drain-to-source current $(I_{DS})^{1/2}$ as a function of the gate voltage (V_g).[60] All FET devices were fabricated by employing the top-contact configuration

(63) Loi, M. A.; Toffanin, S.; Muccini, M.; Forster, M.; Scherf, U.; Scharber, M. *Adv. Funct. Mater.* **2007**, *17*, 2111.

for reducing the contact resistance. The p-type output characteristics of **P4TBT**, **P4TDTBT**, **P4TDTQ**, and **P4TDPP** are shown in Figure 5a−d, which exhibit good current modulation and well-defined linear and saturation regions. In addition, the corresponding transfer characteristics are depicted in Figure S6 of the Supporting Information. The maximum mobilities of the FETs prepared from **P4TBT**, **P4TDTBT**, **P4TDTQ**, and **P4TDPP** using chloroform as the processing solvent are 3.37×10^{-3}, 3.22×10^{-2}, 2.57×10^{-4}, and 1.15×10^{-1} $cm^2\ V^{-1}\ s^{-1}$, respectively, and the on/off ratios ranged from 10^3 to 10^5. The order of polymer FET mobility is consistent with the obtained optical band gap, which indicates the significance of intramolecular charge transfer or polymer chain packing. To further improve the performance, we employed the mixed solvents of 95:5 (v/v) chloroform/chlorobenzene to induce the polymer packing, and the corresponding FET performance is also shown in Table 2. Note the poor film quality of the studied polymer on the ODTS-treated wafer if only high boiling-point solution (chlorobenzene) was used as the processing solvent. The **P4TBT**, **P4TDTQ**, and **P4TDTBT** based FETs prepared by the mixed solvents exhibited moderate enhancement of the characteristics of the carrier mobility and on/off ratio. The high-boiling-point chlorobenzene fraction could reduce the evaporation rate of solvent and further facilitate the packing of polymer chains.

Table 2. FET Characteristics of the 4T-Based Donor−Acceptor Copolymers

solvent[a]	type	mobility ($cm^2\ V^{-1}\ s^{-1}$)	on/off[avg]	V_t^{avg} (V)
		P4TBT		
CF	p	3.37×10^{-3}	7.40×10^5	−2
CF/CB	p	1.31×10^{-2}	1.85×10^7	3
		P4TDTBT		
CF	p	3.22×10^{-2}	4.25×10^5	13
CF	n	2.13×10^{-4}	2.40×10^1	85
CF/CB	p	3.81×10^{-2}	9.97×10^5	15
CF/CB	n	3.17×10^{-4}	6.36×10^4	124
		P4TDTQ		
CF	p	2.57×10^{-4}	1.23×10^3	−39
CF/CB	p	3.10×10^{-4}	7.64×10^4	−2
		P4TDPP		
CF	p	1.15×10^{-1}	2.49×10^4	18
CF	n	1.05×10^{-3}	3.77×10^2	52
CF/CB	p	1.09×10^{-1}	7.03×10^4	−6
CF/CB	n	3.08×10^{-3}	7.34×10^2	95

[a] CF: chloroform. CF/CB: chloroform/chlorobenzene (95:5, v/v).

To further investigate its molecular organization and film morphology of **P4TDPP**, the X-ray diffraction analysis (XRD) was explored. The drop-cast film of **P4TDPP** on the ODTS-modified wafer was prepared from chloroform for X-ray analysis, as shown in Figure 6. The distinct diffraction peak at $2\theta \approx 4.85°$ corresponds to the d_1 spacing value of 18.2 Å, which is assigned to the interchain spacing between polymer main chains, where the alkylthiophene substituents are segregated similar to those of π-conjugated polymers with long side chains.[40,62] The second-order diffraction peak (d_2 = 9.20 Å) which is proportional to d_1 spacing (d_1:$d_2 \sim 2$:1) is also observed

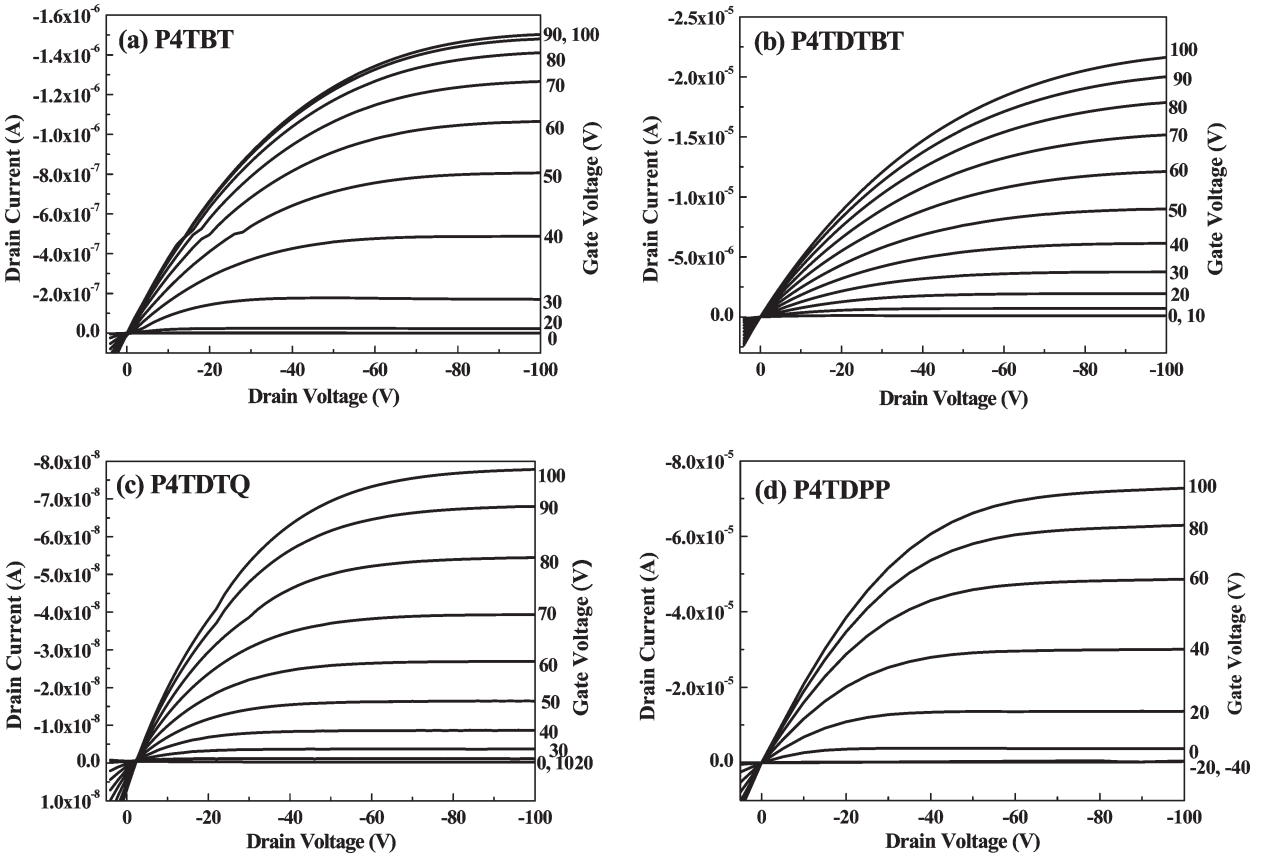

Figure 5. p-Type output characteristics of FETs of (a) **P4TBT**, (b) **P4TDTBT**, (c) **P4TDTQ**, and (d) **P4TDPP** prepared by spin-coating on the ODTS-modified substrates from chloroform/chlorobenzene (95:5, v/v) mixed solvent and annealing at 150 °C for 1 h.

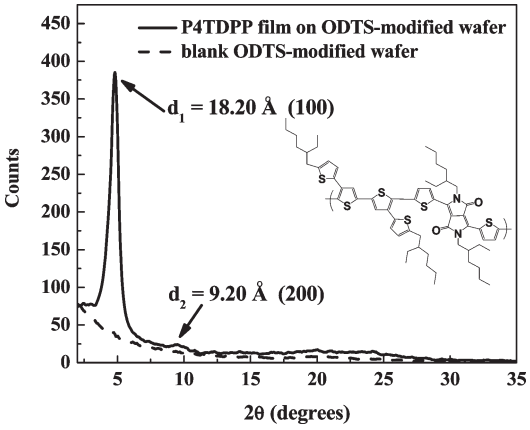

Figure 6. XRD pattern of the **P4TDPP** drop-cast film from the chloroform solution on the ODTS-modified SiO_2 wafer.

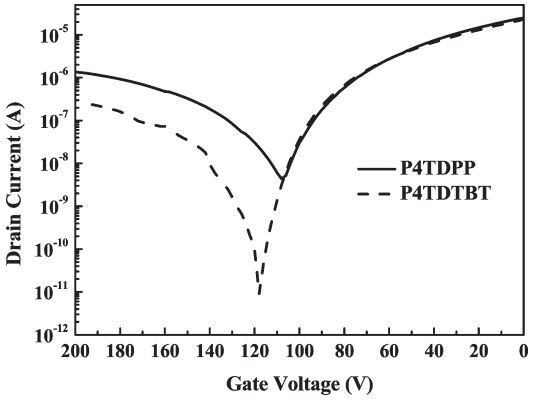

Figure 7. n-Type transfer characteristics of **P4TDTBT** and **P4TDPP** FETs spin-coated on ODTS substrates from the chloroform/chlorobenzene (95:5, v/v) mixed solvent, where $V_{ds} = +60$ V.

in Figure 6, implying a highly organized packing of **P4TDPP**. Hence, the 18.2 Å out of plane spacing (100) in **P4TDPP** film suggests partial interdigitation of the side chains,[35,40,62] indicative of the formation of lamellar structure for enhancing charge transport. It suggests that the crystalline formation of **P4TDPP** attributed to the conjugated thiophene segment as side chain[35] is both confirmed by XRD and DSC for high FET mobility.

Note that the performance of **P4TBT** gave an unexpectedly high mobility of up to 1.31×10^{-2} cm^2 V^{-1} s^{-1} and an on/off ratio of 1.85×10^7 using the mixed solvents, even though its low-lying HOMO energy level is -5.52 eV, which is supposed to result in a large injection barrier of holes between **P4TBT** and gold electrodes. It also could be attributed to the order packing enhancing charge transport manifested in the XRD analysis (Figure S7 in Supporting Information). **P4TBT** exhibits a larger *d* spacing (20.55 Å), lower intensity of diffraction peak, and much low-lying HOMO compared to **P4TDPP**, leading to its lower mobility. It is noted that **P4TBT**, **P4TDTBT**, and **P4TDPP** exhibit much higher hole mobility than **F8BT**,[48] **PFDTBT**,[51] and **PCBTDPP**,[41] respectively, presumably because of the fact that the **4T** building block induces a strong ICT facilitating intramolecular charge transport and, further, the aromatic side chain provides an additional channel for enhancing intermolecular charge transport.

Although there is a large energy barrier between the high-work-function gold electrode and the LUMO levels of the prepared polymers, n-type FET mobilities are observed from **P4TDTBT** and **P4TDPP**, as summarized in Table 2. Figure 7 shows the typical n-type output characteristics of **P4TDTBT** and **P4TDPP** based FET devices, with the maximum electron mobilities of 3.17×10^{-4} and 3.08×10^{-3} cm^2 V^{-1} s^{-1}, respectively, using the gold top-contact electrodes. The drain current is high if $V_g - V_d < V_t$, which is a typical behavior of ambipolar transistors, since the hole current is injected from drain electrodes into the channel.[59] However, the n-type properties of **P4TDTQ** and **P4TBT** are not available, even though aluminum was used as the electrode instead of gold. It is attributed to the influence of the high-lying LUMO levels of **P4TBT** (-3.24 eV) and **P4TDTQ** (-3.22 eV), leading to large energy barriers for electron injection. **P4TDTBT** and **P4TDPP** show considerable average threshold voltages of 52−95 and 85−124 V for n-type behaviors, respectively, which could be attributed to the energy barrier (1.72−1.48 eV) between gold electrode and their LUMO levels as well as electron trapping at the interface between conjugated polymers and SiO_2 substrates.[59] Note that the **P4TDPP** FET device exhibited a high hole mobility of 0.115 cm^2 V^{-1} s^{-1} comparable to the performance of the well-known regioregular P3HT devices.[47] This might be attributed to the influence of intermolecular chain packing enhanced by the coplanar unit of **4T**. In addition, the obtained electron mobility of 3.08×10^{-3} cm^2 V^{-1} s^{-1} is due to its low-lying LUMO level. The ambipolar characteristics of **P4TDPP** could have potential applications as inverters.[45,64]

Air Stability of the FET Device. The air stability of the devices are monitored by measuring hole mobility (μ_h), on/off ratio (I_{on}/I_{off}), and threshold voltage (V_t) as a function of time, as shown in Figure 8. **P4TDTBT** and **P4TDPP** exhibit excellent air stability, and their corresponding mobilities decrease slightly from 3.22×10^{-2} to 2.53×10^{-2} and 1.15×10^{-1} to 4.16×10^{-2} cm^{-2} $V^{-1}s^{-1}$, respectively, after exposure to air for $1^1/_2$ months. Interestingly, the on/off ratio of **P4TDPP** in air compared to that in N_2 increases 2 orders of magnitude to 10^6. It is attributed to the fact that the electron transport of **P4TDPP** is suppressed in air and almost only holes are present under voltage bias, since oxygen and moisture act as electron traps and lead to a low number of electrons in the channel. When the electron mobility drops dramatically upon exposure to the air leading to low off current, the on/off ratio subsequently increases. Thus, **P4TDPP** reveals a high on/off ratio of 10^6 and a low electron mobility of approximately 10^{-7} cm^{-2} V^{-1} s^{-1} in air. The good air-stable performance of **P4TDPP** might be attributed to its high ionization potential and the close packing of polymer chains, avoiding the chemical degradation and the intrusion of oxygen and moisture. On the contrary, the on/off ratios of **P4TDTBT** decreases 3 orders of magnitude in air because of its high-lying

(64) Kim, F. S.; Guo, X. G.; Watson, M. D.; Jenekhe, S. A. *Adv. Mater.* **2010**, *22*, 478.

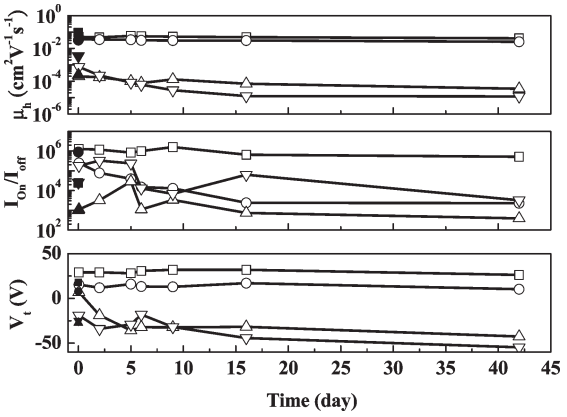

Figure 8. Air-stability testing of FET performance of the polymer films, **P4TBT** (down triangle), **P4TDTBT** (circle), **P4TDTQ** (up triangle), and **P4TDPP** (square), including hole mobility (μ_h), on/off ratio, and threshold voltage (V_t). The solid symbols correspond to an electrical performance in a nitrogen glovebox. Relative humidity ranges from 41% to 60% in air.

HOMO level of −5.04 eV, resulting in unintentional doping.

Polymer Photovoltaic Cell Characteristics. The bulk heterojunction solar cell were fabricated from the studied polymers with a sandwich configuration of ITO/PEDOT:PSS/polymer:$PC_{71}BM$/Ca (30 nm)/Al (100 nm). The active layers of studied polymers devices were prepared without an annealing process. After encapsulation with UV-curing glue, the $I-V$ characteristics were measured in air. The $I-V$ characteristics of polymer solar cell prepared from the blends of polymer:$PC_{71}BM$ (1:3) using the *o*-dichlorobenzene processing solvent are depicted in Figure 9. The photovoltaic properties including open-circuit voltage (V_{oc}), short-circuit current (J_{sc}), fill factor (FF), and power conversion efficiency (PCE) are summarized in Table 3. The **P4TBT**, **P4TDTBT**, **P4TDTQ**, and **P4TDPP** based devices (polymer/$PC_{71}BM$ = 1:3) exhibit the highest PCEs of 1.39%, 1.28%, 1.29%, 1.67%, respectively, based on similar film thickness of ~80 nm. As shown in Table 3, the V_{oc} of the photovoltaic devices increases from 0.57 V (**P4TDTBT**) to 0.64 V (**P4TDPP**), 0.69 V (**P4TDTQ**), and 0.90 V (**P4TBT**). In general, a higher V_{oc} could result from the lower HOMO energy levels of the studied copolymers because V_{oc} is related to the energy differences between the HOMO of the donor (conjugated polymer) and the LUMO of the acceptor ($PC_{71}BM$).[65] The **P4TDTBT** shows a higher hole mobility and absorption coefficient than **P4TBT**, leading to the higher J_{sc}. However, the slightly higher PCE of **P4TBT**-based device could be attributed to the much lower HOMO level, which results in a larger V_{oc} (0.90 V). Moreover, the **P4TDPP** makes the best photovoltaic cell performance among the studied copolymers because of its highest hole mobility, desirable absorption coefficient to better overlap solar spectrum, suitable energy level alignment for high V_{oc}, and efficient charge separation

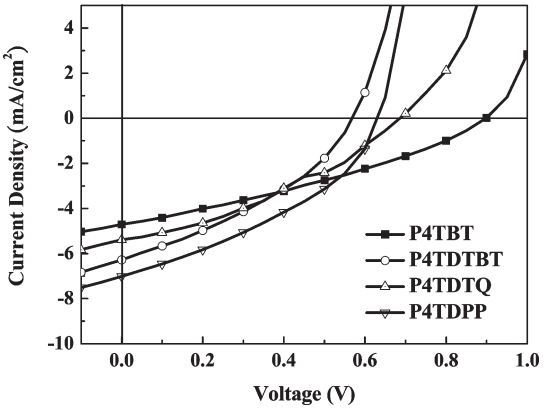

Figure 9. Current density−potential characteristics of polymer solar cells with polymer/$PC_{71}BM$ under the illumination with AM 1.5G solar simulated light (100 mW/cm^2).

Table 3. Photovoltaic Characteristics of the Studied 4T-Based Copolymers/$PC_{71}BM$ (= 1:3) Devices

polymer/$PC_{71}BM$ (1:3)	J_{sc} (mW/cm^2)	V_{oc} (V)	FF	PCE[a] (%)
P4TBT	4.71	0.90	0.33	1.39
P4TDTBT	6.28	0.57	0.36	1.28
P4TPDTQ	5.39	0.69	0.35	1.29
P4TDPP	7.02	0.64	0.37	1.67

[a] The average value of power conversion efficiency is calculated from four pixels in the device.

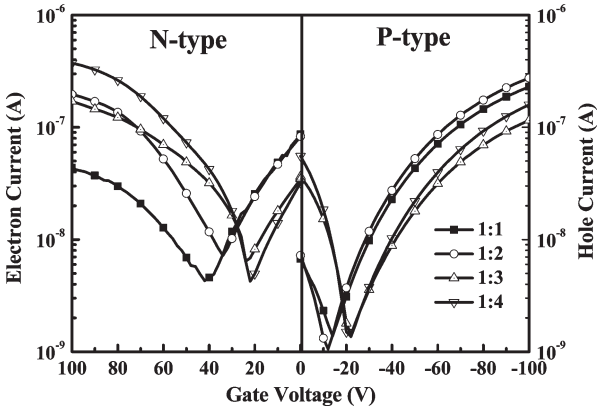

Figure 10. p-Type and n-type transfer characteristics measured from **P4TDPP** blended with various content of $PC_{71}BM$, where V_{ds} = ± 60 V. The devices were prepared by spin coating on PTS substrates.

(the suitable energy differences between the LUMO of the donor and the LUMO of the acceptor is 0.3 eV[66,67]). Hence, we take **P4TDPP** for further investigation on its photovoltaic device.

Since the charge transport in polymer blends is crucial for solar cells, FETs are a powerful tool to investigate the hole and electron mobilities of polymer blends.[61,62] Figure 10 shows the FET mobilities of **P4TDPP** blending with various contents of $PC_{71}BM$, and the corresponding FET and photovoltaic values are listed in Table 4.

(65) Gadisa, A.; Svensson, M.; Andersson, M. R.; Inganas, O. *Appl. Phys. Lett.* **2004**, *84*, 1609.
(66) Scharber, M. C.; Wuhlbacher, D.; Koppe, M.; Denk, P.; Waldauf, C.; Heeger, A. J.; Brabec, C. L. *Adv. Mater.* **2006**, *18*, 789.
(67) Koster, L. J. A.; Mihailetchi, V. D.; Blom, P. W. M. *Appl. Phys. Lett.* **2006**, *88*, 093511.
(68) Zoombelt, A. P.; Mathijssen, S. G. J.; Turbiez, M. G. R.; Wienk, M. M.; Janssen, R. A. J. *J. Mater. Chem.* **2010**, *20*, 2240.

Table 4. FET Carrier Mobilities on the PTS-Treated Substrates and Photovoltaic Characteristics of the Different Ratios of the P4TDPP/$PC_{71}BM$ Blends

P4TDPP/$PC_{71}BM$	hole mobility[a] (μ_h, $cm^2\ V^{-1}\ s^{-1}$)	electron mobility[b] (μ_e, $cm^2\ V^{-1}\ s^{-1}$)	μ_h/μ_e	J_{sc} (mW/cm^2)	V_{oc} (V)	FF	PCE[c] (%)
1:0	3.95×10^{-3}	5.18×10^{-6}					
0:1		1.70×10^{-3}					
1:1	3.37×10^{-4}	4.35×10^{-5}	7.75	5.16	0.61	0.40	1.27
1:2	4.20×10^{-4}	2.83×10^{-4}	1.48	8.05	0.65	0.46	2.43
1:3	1.75×10^{-4}	1.15×10^{-4}	1.52	7.02	0.64	0.37	1.67
1:4	2.57×10^{-4}	4.71×10^{-4}	0.55 (μ_e/μ_h = 1.83)	6.79	0.67	0.37	1.65

[a] Average hole mobility. [b] Average electron mobility. [c] The average value of power conversion efficiency is calculated from four pixels in the device.

Attempting to understand the balance between hole and electron mobilities within polymer blends, phenyltrichlorosilane (PTS) treated substrates were employed to fabricate FET of polymer blends because of its good wetting ability for both **P4TDPP** and $PC_{71}BM$. Even though the choice of the ODTS-treated substrates consistently exhibits better performance in FETs than that from PTS-treated substrates, it is difficult for $PC_{71}BM$ to stick on the ODTS-treated surface. The average hole and electron mobilities of **P4TDPP** FETs are 3.95×10^{-3} and 5.18×10^{-6} $cm^2\ V^{-1}\ s^{-1}$, while the average electron mobility of $PC_{71}BM$ was 1.70×10^{-3} $cm^2\ V^{-1}\ s^{-1}$ on the PTS-treated substrates. The balanced electron and hole mobilities of the **P4TDPP**/$PC_{71}BM$ blends could be obtained in the weight ratios of 1:2, which is in agreement with the highest PCE of 2.43% (V_{oc} = 0.65 V, J_{sc} = 8.05 mA/cm^2, FF = 0.46) of the **P4TDPP**/$PC_{71}BM$ (=1:2) photovoltaic cell device. The above result suggests that the balance of hole and electron mobilities is a key factor for the efficient collection of photogenerated charges in solar cells.[61,62] The lower weight ratios of $PC_{71}BM$ in **P4TDPP**/$PC_{71}BM$ (=1:1) device leads to reduction in the J_{sc} value, due the inefficient charge separation and electron transporting properties (hole mobility $\gg$ electron mobility). Note that the increase of an order of magnitude on the electron mobility is found from the ratio of **P4TDPP**/$PC_{71}BM$ from 1:1 to 1:2. It probably originated from the fact that the network structure of $PC_{71}BM$ starts to be built in this ratio. However, the **P4TDPP**/$PC_{71}BM$ (1:4) device reveals the lower J_{sc} and PCE compared to the **P4TDPP**/$PC_{71}BM$ (1:2), which could be attributed to the decreased absorptive polymer and unbalanced transport mobility of the former (hole mobility < electron mobility). The above result demonstrates the significance of the balance of the hole/electron mobility for photovoltaic cell performance.

Conclusions

We have successfully synthesized four two-dimensional **4T**−acceptor conjugated copolymers by palladium(0)-catalyzed Stille coupling reaction under microwave heating. The results revealed that the electronic structures were readily tuned by copolymerizing with different conjugated electron-accepting units. The optical band gaps (eV) of the studied conjugated copolymers were in the order of **P4TDPP** (1.29) < **P4TDTBT** (1.60) < **P4TDTQ** (1.83) < **P4TBT** (1.88). The high hole mobilities of studied polymers (10^{-1}−10^{-4} $cm^2\ V^{-1}\ s^{-1}$) are mainly due to the enhanced ordered intermolecular packing characteristics in the solid state. On the other hand, the FET electron mobilities were observed for **P4TDTBT** and **P4TDPP**, due to their relatively low-lying LUMO level suitable for electron injection. In particular, **P4TDPP** showed ambipolar characteristics with high hole and electron mobilities. The power conversion efficiency (PCE) could be enhanced up to 2.43% of **P4TDPP**/$PC_{71}BM$ (=1:2) based photovoltaic cells resulting from the balanced hole/electron mobilities. The above results indicate that these two-dimensional **4T**−acceptor conjugated copolymers could enhance the charge-transport characteristics and are promising materials for organic optoelectronic devices.

Acknowledgment. The financial support from National Science Council of Taiwan, Ministry of Economics Affairs of Taiwan, and National Taiwan University Excellent Research program is highly appreciated.

Supporting Information Available: ^1H NMR spectra of monomer **4T** and studied polymers **P4TBT**, **P4TDTBT**, **P4TDTQ**, and **P4TDPP**; TGA curves of studied copolymers at a heating rate of 20 °C/min under a nitrogen atmosphere; p-type transfer characteristics curve of FETs of **P4TBT**, **P4TDTBT**, **P4TDTQ**, and **P4TDPP**; XRD pattern of the **P4TBT** drop-cast film from the chloroform solution on the ODTS-modified SiO_2 wafer; the effect of different surface treatments on poly(**4T**−acceptor) (PDF). This material is available free of charge via the Internet at http://pubs.acs.org.